PHYSICAL REVIEW B **77**, 045316 (2008)

Determination of the branch-point energy of InN: Chemical trends in common-cation and common-anion semiconductors

P. D. C. King, T. D. Veal, P. H. Jefferson, S. A. Hatfield, L. F. J. Piper,* and C. F. McConville†
Department of Physics, University of Warwick, Coventry, CV4 7AL, United Kingdom

F. Fuchs, J. Furthmüller, and F. Bechstedt
Institut für Festkörpertheorie und -optik, Friedrich-Schiller-Universität, Max-Wien-Platz 1, D-07743 Jena, Germany

Hai Lu‡ and W. J. Schaff
Department of Electrical and Computer Engineering, Cornell University, Ithaca, New York 14853, USA
(Received 28 September 2007; published 16 January 2008)

Bulk and surface electronic properties of Si-doped InN are investigated using high-resolution x-ray photoemission spectroscopy, optical absorption spectroscopy, and quasiparticle corrected density functional theory calculations. The branch point energy in InN is experimentally determined to lie 1.83 ± 0.10 eV above the valence-band maximum. This high position relative to the band edges is used to explain the extreme fundamental electronic properties of the material. Far from being anomalous, these properties are reconciled within chemical trends of common-cation and common-anion semiconductors.

DOI: 10.1103/PhysRevB.77.045316 PACS number(s): 71.55.Eq, 73.61.Ey, 78.20.−e, 79.60.−i

I. INTRODUCTION

Indium nitride (InN) remains one of the least understood of the III-V semiconductor systems, despite considerable recent research in this area.[1,2] The material presents enormous potential for device applications ranging from terahertz emission[3] to chemical sensing[4] and high-efficiency radiation-hard solar cells.[5] However, InN has a number of striking fundamental properties. In particular, InN is known to exhibit electron accumulation at its surface,[6,7] which is much more extreme than in InAs,[8,9] the only other III-V material in which this phenomenon has been observed. Electron accumulation is also present at the surface of *p*-type InN, resulting in the formation of a surface inversion layer[2] which masks the bulk *p*-type conductivity. Additionally, InN has a propensity for high *n*-type conductivity,[10] with nominally undoped material typically having carrier concentrations in the range $10^{17}-10^{21}$ cm^{-3}. Possible implementation of device applications relies upon a significantly improved understanding and ability to control these material properties.

The branch point energy, which constitutes a charge neutrality level for the semiconductor and is thought to be universal on an absolute energy scale,[11] marks the energy where surface states change their character from predominantly donor type (below) to predominantly acceptor type (above).[12] Additionally, within the amphoteric defect model (ADM),[13] it marks the energy at which the formation of donor (below) or acceptor (above) native defects becomes favorable. More generally, the branch point determines the favorable charge state of all gap states including surface states, metal- and interface-induced gap states, and defect-induced gap states. Thus, its position relative to the band edges in the material is crucial in determining fundamental bulk and surface electronic properties such as surface space charge characteristics, doping limits, and metal/semiconductor contact characteristics.

This paper reports an investigation into the branch point energy in InN by studies of Si-doped InN samples (and an undoped reference sample) using a combination of high-resolution x-ray photoemission spectroscopy (XPS), optical absorption spectroscopy (OAS), and theoretical calculations employing quasiparticle corrected density functional theory (QPC-DFT). Its extreme location, determined as lying 1.83 ± 0.10 eV above the valence-band maximum (VBM), is rationalized within chemical trends.

II. EXPERIMENTAL AND THEORETICAL DETAILS

The InN samples were grown on *c*-plane sapphire substrates by plasma-assisted molecular-beam epitaxy. Details of the growth are reported elsewhere.[14] The InN layer thicknesses ranged from 250 to 2000 nm and the growth temperature was ~480 °C. The carrier concentrations and mobilities (from single-field Hall effect measurements) vary from 2.0×10^{18} to 6.6×10^{20} cm^{-3} and 1100 to 38 cm^2 V^{-1} s^{-1}, respectively. All except the lowest carrier concentration sample were doped with Si.

The XPS measurements were performed using a Scienta ESCA300 spectrometer at the National Centre for Electron Spectroscopy and Surface Analysis, Daresbury Laboratory, UK. x rays, of energy $h\nu = 1486.6$ eV, were produced using a monochromated rotating anode Al $K\alpha$ x-ray source. The ejected photoelectrons were analyzed by a 300 mm mean radius spherical-sector electron energy analyzer with 0.8 mm slits at a pass energy of 150 eV. The effective instrumental resolution is 0.45 eV derived from the Gaussian convolution of the analyzer broadening and the natural linewidth of the x-ray source (0.27 eV). The binding energy scale is given with respect to the Fermi level and was calibrated using the Fermi edge of an ion-bombarded silver reference sample that is regularly used to calibrate the spectrometer. The optical absorption measurements were performed using a Perkin-Elmer Lambda 25 UV-visible spectrometer and a Perkin-Elmer Spectrum GX Fourier transform infrared spectrometer for energies above and below 1.2 eV, respectively.

 ©2008 The American Physical Society

The QPC-DFT calculations were performed using the hybrid functional HSE03 for exchange and correlation.[15] The electron-ion interaction was treated in the framework of the projector-augmented wave method, taking into account the In 4*d* electrons as valence states. Quasiparticle effects were included in the calculation of the density of states by a G_0W_0 correction of the HSE eigenvalues. Details of the calculations are reported elsewhere.[16] For comparison with the experimental results, the QPC-DFT density of states is broadened by a 0.2 eV full width at half maximum (FWHM) Lorentzian and a 0.45 eV FWHM Gaussian to account for lifetime and instrumental broadening, respectively.

III. RESULTS AND ANALYSIS

The carrier concentration, from single-field Hall effect measurements, increases with increasing Si-cell temperature during growth, indicating that Si is being incorporated into the InN host and is electrically active, acting as a donor. This is confirmed by XPS measurements of the Si 2*p* core-level peak (not shown), which increases in intensity with increasing carrier concentration. Additionally, the binding energy of the peak (~102 eV) is indicative of Si-N bonding[17] (the peak is chemically shifted from its elemental position in Si of ~99 eV), confirming that the Si preferentially occupies the In site, therefore acting as a donor.

XPS was employed to determine the pinning position of the surface Fermi level as a function of bulk carrier concentration; the leading edges of the valence-band photoemission spectra are shown in Fig. 1(a). Increasing the doping shifts the leading edge of the valence-band photoemission to higher binding energies, indicating an increase in the VBM to Fermi level separation at the surface. The surface Fermi level position can be obtained by extrapolating the leading edge of the valence-band photoemission to the baseline in order to take account of the finite resolution of the spectrometer.[18] The values determined in this way are shown in Fig. 1(b), revealing a stabilization of the surface Fermi level at 1.83±0.10 eV above the VBM with increasing doping.

For low bulk doping levels in the presence of significant band bending, this method of analysis is known to underestimate the VBM to surface Fermi level separation.[19] The high energy of the incident photons in XPS measurements allows accurate comparison between the valence-band photoemission spectra and theoretical calculations of the valence-band density of states (VB-DOS).[20] As an alternative method of analysis, the valence-band photoemission spectra can be compared to theoretical calculations of the VB-DOS, and the shift of energy between the lowest energy peak in the VB-DOS (with the VBM defined at 0 eV) and the corresponding peak in the XPS spectra gives the VBM to surface Fermi level separation. The valence-band XPS spectra are shown, compared to the QPC-DFT VB-DOS, in Fig. 2(a).

The VBM to surface Fermi level separation determined by this method is shown in Fig. 3(a). For the lowest carrier concentration sample, the Fermi level is pinned somewhat higher at the surface than was determined using the linear extrapolation method due to the significant downward band

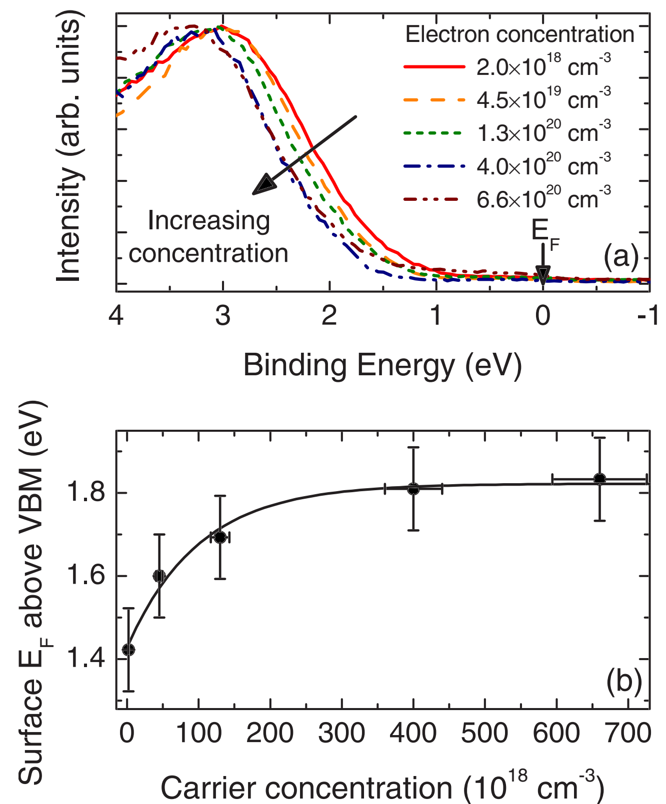

FIG. 1. (Color online) (a) Valence-band photoemission spectra and (b) corresponding VBM to surface Fermi level separation evaluated by extrapolating the leading edge of the XPS spectra to the baseline to account for the finite resolution of the spectrometer. The solid line is an exponential fit to the data to guide the eye.

bending present and the finite escape depth of photoelectrons.[19] The surface Fermi level positions for the higher carrier concentration samples agree within experimental error between the two methods of analysis. For the two lowest carrier concentration samples, this analysis reveals that the surface Fermi level is virtually static with increasing carrier concentration. Further increase in carrier concentration again reveals an increase and then saturation in the surface Fermi level position.

Additionally, OAS spectra [Fig. 2(b)] indicate the effects of doping on the bulk Fermi level. In the low energy part of the spectrum, the increase in the absorption with doping is attributed to an increase in free-carrier absorption. In the higher energy part of the spectrum, a significant increase in the absorption edge energy is observed; this is attributed to the Burstein-Moss (or band-filling) effect,[21,22] whereby the (degenerate) Fermi level shifts to higher energies with increasing doping, represented schematically in the inset of Fig. 2(b). Additionally, an exponential Urbach tail is seen below this absorption edge, and the extent of this tail increases with doping concentration due to the increase in band-tailing effects.

The bulk Fermi level position can be determined from the electron concentration in the samples and carrier statistics calculations. However, due to the very high doping levels involved, common band structure approximations (such as the $\mathbf{k}\cdot\mathbf{p}$ model) are no longer valid. Consequently, the

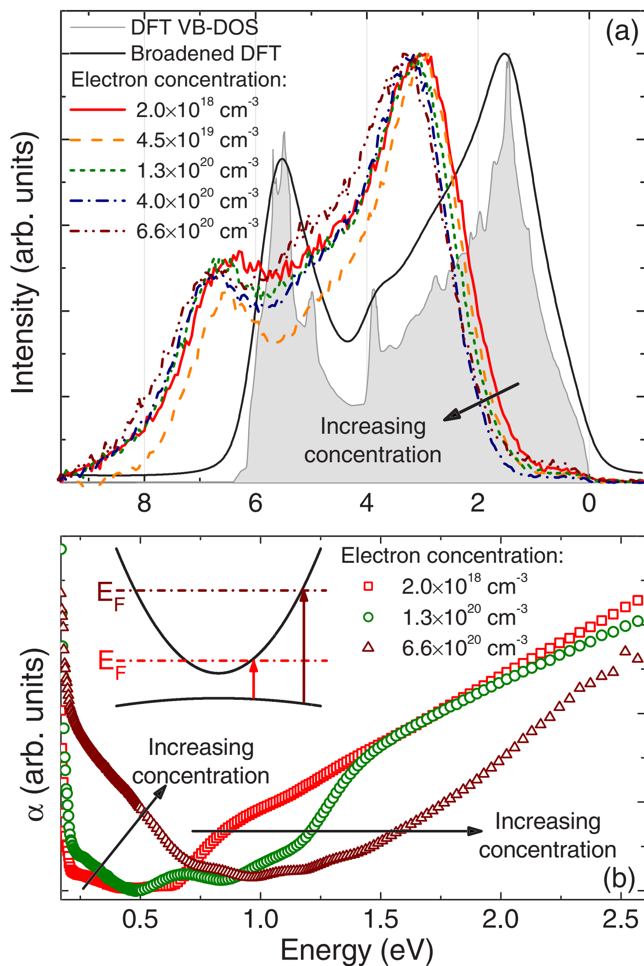

FIG. 2. (Color online) (a) QPC-DFT VB-DOS shown without (shaded) and with lifetime and instrumental broadening and the Shirley-background-subtracted valence-band photoemission spectra, offset from the QPC-DFT due to Fermi level shifts, and (b) optical absorption coefficient α of three samples showing clear Burstein-Moss shift with change in Fermi level E_F represented schematically in the inset.

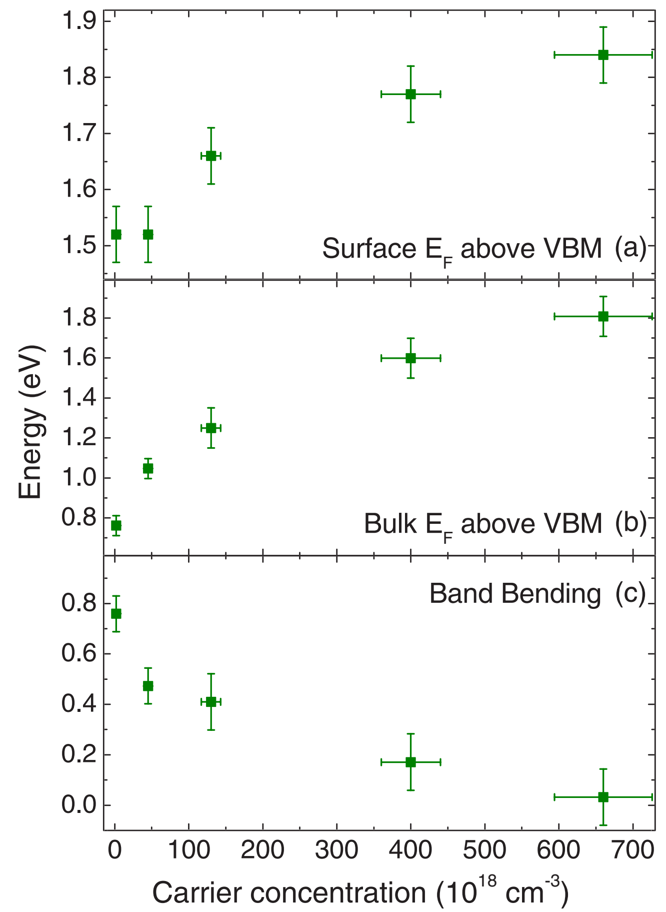

FIG. 3. (Color online) (a) VBM to surface Fermi level E_F separation determined from the XPS measurements, (b) VBM to bulk Fermi level separation determined numerically from the conduction-band dispersion of the QPC-DFT band structure, and (c) resulting band bending as a function of carrier concentration.

conduction-band dispersion from QPC-DFT calculations has been employed to determine the bulk Fermi levels from the carrier concentrations; these are shown in Fig. 3(b). It should be noted that the electron concentrations determined from the single-field Hall effect measurements contain a contribution from the surface electron accumulation region in addition to the bulk.[23] This introduces a small error in calculation of the bulk Fermi level based on the single-field Hall effect concentrations, as represented by the error bars in Fig. 3(b).

Initially, an increase in carrier concentration leads to a rapid increase in bulk Fermi level [Fig. 3(b)], although the rate of this reduces with increasing carrier concentration. Any difference between the bulk and surface Fermi level positions must be incorporated via a bending of the bands relative to the Fermi level [Fig. 3(c)], which tends smoothly to zero with increasing bulk carrier concentration.

IV. DISCUSSIONS

For a given bulk Fermi level, the surface Fermi level position is determined by the considerations of charge neutrality. If the surface Fermi level is located below the branch point, some donor surface states will be unoccupied and hence positively charged. This surface charge must be balanced by a space charge due to downward band bending, leading to an increase in the near-surface electron density (an accumulation layer).

For nominally undoped (low carrier concentration) InN, the downward band bending is extreme, resulting in the observed[7] large accumulation of electrons at the surface. For initial increases in bulk Fermi level, the change in the space charge can be accommodated by very small shifts in the surface Fermi level position; the Fermi level is strongly *pinned* at the surface. This is seen by the virtually static position of the surface Fermi level for the two lowest carrier concentration samples in Fig. 3(a). However, as the bulk Fermi level increases further, the reduction in band bending means that the space charge is no longer sufficient to balance the surface state charge, causing the Fermi level to move closer to the branch point at the surface in order that fewer donor surface states are unoccupied, reducing the surface state charge. As the bulk Fermi level approaches the branch point, the surface Fermi level must also therefore approach the branch point, causing the band bending to tend to zero.

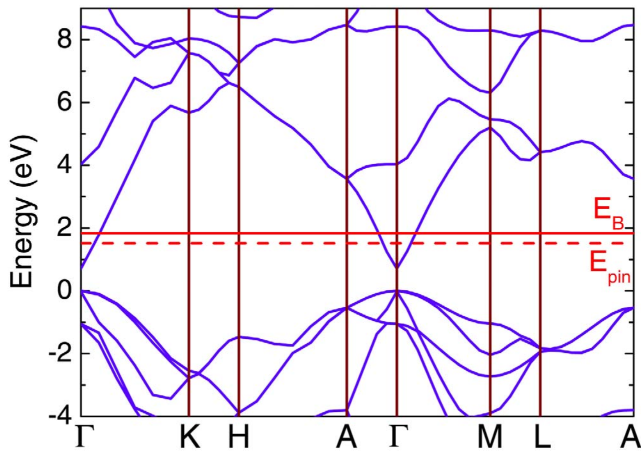

FIG. 4. (Color online) QPC-DFT band structure across the Brillouin zone with the determined branch point E_B and surface Fermi level pinning E_{pin} positions.

The stabilization of the Fermi level at the branch point can be understood within the ADM. When the bulk Fermi level is well below the branch point, Si preferentially occupies the In site (Si_{In}^{+}), acting as a donor, and any native defects preferentially have donor character, increasing the bulk conductivity. As the Fermi level increases, acceptor defects such as triply charged In vacancies (V_{In}^{3-}), Si on the N site (Si_{N}^{-}), and acceptor-type defect complexes become more favorable, preventing further increase in Fermi level and acting to stabilize it at the branch point. In vacancies have previously been observed to provide partial compensation in Si-doped InN.[24] Additionally, the low measured mobilities (by the single-field Hall effect) and large Urbach tailing observed in the most heavily doped samples [Fig. 2(b)] suggest the presence of significant numbers of compensating native defects and impurities in the material.

Both methods of analysis of the XPS data presented above reveal a stabilization with heavy doping of the surface Fermi level at 1.83 ± 0.10 eV: The branch point energy is therefore determined as lying 1.83 ± 0.10 eV above the VBM, as illustrated in Fig. 4, slightly above the pinning position for moderately doped samples. In particular, the linear extrapolation method of analysis (Fig. 1) allows a direct experimental determination of the branch point energy without recourse to theoretical calculations or knowledge of the bulk Fermi level in the samples.

The branch point is located close to the average midgap energy across the entire Brillouin zone.[12] Tersoff[25] identified an appropriate average midgap energy as

$$E_0 \approx \frac{1}{2}(\bar{E}_V + \bar{E}_C), \quad (1)$$

where $\bar{E}_V = E_V - \frac{1}{3}\Delta_{so}$ is the position of the "effective" valence-band maximum in the absence of spin-orbit splitting and $\bar{E}_C$ is the indirect conduction-band minimum. From the QPC-DFT band structure calculations (Fig. 4), taking the conduction-band energy at the A point for $\bar{E}_C$, the branch point would be expected, from Eq. (1), to be close to 1.78 eV above the VBM, in agreement with the measured value. From Fig. 4, the conduction-band energy at the Γ point is significantly lower than the average band-edge across the Brillouin zone: The branch point in InN therefore lies well above the conduction-band minimum (CBM), in contrast to almost all other III-V semiconductors where the branch point is located below the CBM. This can be understood within chemical trends, as discussed in Section V.

The branch point energy determined here also agrees very well with previous theoretical calculations. Van de Walle and Neugebauer[11] located the branch point at 1.88 eV above the VBM in InN using *ab initio* calculations. Additionally, Green's functions calculations by Robertson and Falabretti[26] give a branch point 1.87 eV above the VBM, and they also determined a value of 1.88 eV using the theoretical calculations of Wei and Zunger.[27]

V. CHEMICAL TRENDS

The unusually high location of the branch point energy relative to the CBM in InN compared to other III-V semiconductors can be explained within chemical trends by considering the band alignment of the common-anion III-N and the common-cation In-V compounds, shown in Fig. 5(a). Appealing to a simple tight-binding model, the valence (conduction) band edge derives mainly from the bonding (antibonding) state of anion and cation p (s) orbitals.[32] Due to the very small energy differences in the cation p orbitals [Fig. 5(b)], the predominant factor in determining the valence-band edge variation in the III-Ns is the interaction between the cation d orbitals and the N $2p$ orbital:[33] This p-d repulsion pushes the VBM up in GaN and InN (the Ga $3d$ and In $4d$ orbitals are located below the VBM and hybridize with the N $2s$ orbital) with respect to AlN. The reduction of the CBM with increasing cation atomic number results from the change in cation s-orbital energy coupled with a decrease in the s-s repulsion strength between the cation and anion s orbitals with increasing cation-anion bond length (on moving from AlN to InN). Similar considerations hold for the common-cation compounds. The VBM follows the trend of the anion p orbitals, causing a lowering of the band edge energy with decreasing anion atomic number. Furthermore, the spin-orbit splitting (which pushes the VBM upward in energy) decreases with decreasing anion atomic number. The movement of the CBM results from the combined effects of the anion s-orbital energy shifts [Fig. 5(b)] and the change of s-s coupling with cation-anion bond length and energy separation of the In $5s$ and anion s orbitals. In particular, the very low position of the CBM in InN results from the low energy of the N $2s$ orbital and the large In-N bond length.

The position of InN, lying at the intersection of these chemical trends, results in its extreme properties, with a narrow band gap and CBM located extremely low with respect to the branch point. This explains the propensity for high unintentional n-type conductivity in InN: Within the ADM, when the bulk Fermi level lies below the branch point, donor-type native defects are most favorable, tending to increase the Fermi level toward the branch point. Conversely,

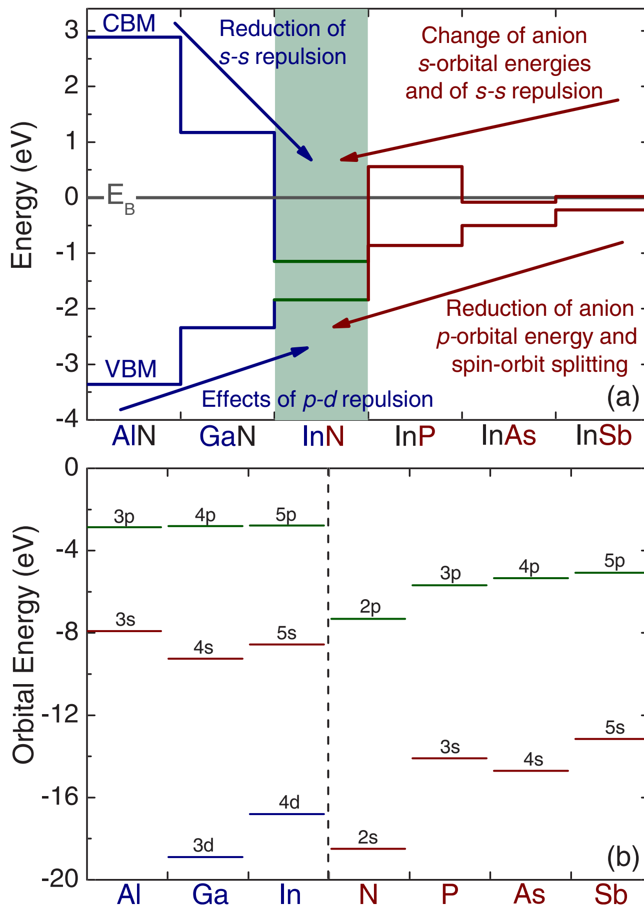

FIG. 5. (Color online) (a) Band lineups relative to the branch point energy in InN and common-cation and common-anion semiconductors determined from experimentally measured valence-band offsets (Refs. 28 and 29) and experimentally (this study) and theoretically (Ref. 30) determined values of the branch point energy position. (b) The locations of the constituent atom orbital energies, taken from Wei *et al.* (Ref. 31), and anion-cation state coupling explain the chemical trends in the band offsets.

for bulk Fermi levels above the branch point, acceptor-type native defects have the lower formation energies, tending to reduce the net electron concentration and lower the Fermi level toward the branch point. The high branch point energy relative to the CBM in InN means that unintentional native defects will preferentially form as donors, generally resulting in a high unintentional n-type bulk conductivity. These effects are also responsible for the observed stabilization of the Fermi level when InN is irradiated with high energy particles.[34]

Although the zero temperature InN band gap is now generally accepted to be ~0.7 eV,[35] it was previously thought to be ~1.9 eV.[36] These early measurements were largely performed by OAS on sputter grown InN samples, which are likely to contain many native defects driving the Fermi level toward the branch point. A Burstein-Moss shift to the branch point energy determined here is an important factor in explaining these previously observed high optical gap values.

Due to the high location of the branch point relative to the CBM, the Fermi level at the surface is pinned below the branch point, resulting in downward band bending and the observed electron accumulation.[7] The position of the branch point energy is a bulk band structure property, explaining the universality of the electron accumulation observed at both polarities of c-plane and at a-plane InN surfaces.[37] Additionally, due to the similar surface Fermi level pinning position in p-type InN,[19] intrinsic electron accumulation is also present in p-type samples,[2] resulting in a surface electron layer separated from the bulk p-type region by a hole depletion layer.

This is very similar to the situation in InAs, where the branch point is also located above the CBM [Fig. 5(a)], and electron accumulation (inversion) layers are present at n-type (p-type) surfaces. However, due to the smaller separation between the CBM and the branch point energy in InAs than in InN, the surface state densities are significantly lower in the former material,[7,9] and so the electron accumulation is less extreme. In contrast, in GaN, for example, the branch point energy is located significantly below the CBM, and so the surface Fermi level will tend to be pinned below (above) the bulk Fermi level for n-type (p-type) material. Consequently, electron (hole) depletion layers are observed at the surface of n-type (p-type) material.[38] A smooth transition occurs between the space-charge regions of InN and GaN for both n- and p-type bulk conductivities.[19,39]

Far from being anomalous, therefore, the fundamental electronic properties of InN are governed by the same overriding mechanism as in other semiconductors, namely, the position of the band edges relative to the branch point energy. The extreme nature of InN can be rationalized by the high branch point energy relative to the band edges. This position follows from the chemical trends of common-cation and common-anion semiconductors.

VI. CONCLUSIONS

In conclusion, we have shown that the branch point energy in InN is located 1.83 ± 0.10 eV above the valence-band maximum, well above the Γ-point conduction-band minimum in InN. This was determined directly from experimental energy measurements (from x-ray photoemission spectroscopy) of the surface Fermi level position stabilized at the branch point by heavy Si doping and confirmed using a combination of photoemission measurements and quasiparticle corrected density functional theory calculations.

Many of the fundamental properties of the material which are often considered unusual, such as an extreme electron accumulation at the surface, inversion layer formation at the surface of p-type material, and the propensity for high unintentional n-type conductivity, were explained by the position of the branch point energy relative to the band edges. Far from being anomalous, these properties and the location of the branch point significantly above the Γ-point CBM were explained within chemical trends of the common-cation and common-anion III-V semiconductors.

ACKNOWLEDGMENTS

We are grateful to Danny Law and Graham Beamson of NCESS for their assistance with XPS measurements. Also, we acknowledge the Engineering and Physical Sciences Research Council, UK, for financial support under Grant No. EP/C535553/1 and access to the NCESS facility under Grant No. GR/S14252/01 and the Deutsche Forschungsgemeinschaft for financial support under Project No. Be1346/18-2.

*Present address: Department of Physics, Boston University, Boston, MA 02215, USA.

†Corresponding author: c.f.mcconville@warwick.ac.uk

‡Present address: Department of Physics, Nanjing University, Nanjing, 210093, China.

[1] L. Colakerol, T. D. Veal, H.-K. Jeong, L. Plucinski, A. DeMasi, T. Learmonth, P.-A. Glans, S. Wang, Y. Zhang, L. F. J. Piper, P. H. Jefferson, A. Fedorov, T.-C. Chen, T. D. Moustakas, C. F. McConville, and K. E. Smith, Phys. Rev. Lett. **97**, 237601 (2006).

[2] R. E. Jones, K. M. Yu, S. X. Li, W. Walukiewicz, J. W. Ager III, E. E. Haller, H. Lu, and W. J. Schaff, Phys. Rev. Lett. **96**, 125505 (2006).

[3] R. Ascázubi, I. Wilke, K. Denniston, H. Lu, and W. J. Schaff, Appl. Phys. Lett. **84**, 4810 (2004).

[4] H. Lu, W. J. Schaff, and L. F. Eastman, J. Appl. Phys. **96**, 3577 (2004).

[5] J. Wu, W. Walukiewicz, K. M. Yu, W. Shan, J. W. Ager III, E. E. Haller, H. Lu, W. J. Schaff, W. K. Metzger, and S. Kurtz, J. Appl. Phys. **94**, 6477 (2003).

[6] H. Lu, W. J. Schaff, L. F. Eastman, and C. E. Stutz, Appl. Phys. Lett. **82**, 1736 (2003).

[7] I. Mahboob, T. D. Veal, C. F. McConville, H. Lu, and W. J. Schaff, Phys. Rev. Lett. **92**, 036804 (2004).

[8] D. C. Tsui, Phys. Rev. Lett. **24**, 303 (1970).

[9] M. Noguchi, K. Hirakawa, and T. Ikoma, Phys. Rev. Lett. **66**, 2243 (1991).

[10] A. G. Bhuiyan, A. Hashimoto, and A. Yamamoto, J. Appl. Phys. **94**, 2779 (2003).

[11] C. G. Van de Walle and J. Neugebauer, Nature (London) **423**, 626 (2003).

[12] W. Mönch, *Semiconductor Surfaces and Interfaces* (Springer, Berlin, 2001).

[13] W. Walukiewicz, J. Vac. Sci. Technol. B **5**, 1062 (1987).

[14] W. J. Schaff, H. Lu, L. F. Eastman, W. Walukiewicz, K. M. Yu, S. Keller, S. Kurtz, B. Keyes, and L. Gevilas, in *State-of-the-Art Program on Compound Semiconductors XLI and Nitride and Wide Bandgap Semiconductors for Sensors, Photonics, and Electronics V*, The Electrochemical Society Proceedings Series, Honolulu, HI, 2004, edited by H. M. Ng and A. G. Baca (Electrochemical Society, Pennington, NJ, 2004), Vol. 2004-06, pp. 358–371.

[15] J. Heyd, G. E. Scuseria, and M. Ernzerhof, J. Chem. Phys. **118**, 8207 (2003).

[16] F. Fuchs, J. Furthmüller, F. Bechstedt, M. Shishkin, and G. Kresse, Phys. Rev. B **76**, 115109 (2007).

[17] J. Finster, E. D. Klinkenberg, J. Heeg, and W. Braun, Vacuum **41**, 1586 (1990).

[18] S. A. Chambers, T. Droubay, T. C. Kaspar, and M. Gutowski, J. Vac. Sci. Technol. B **22**, 2205 (2004).

[19] P. D. C. King, T. D. Veal, P. H. Jefferson, C. F. McConville, H. Lu, and W. J. Schaff, Phys. Rev. B **75**, 115312 (2007).

[20] L. Ley, R. A. Pollak, F. R. McFeely, S. Kowalczyk, and D. A. Shirley, Phys. Rev. B **9**, 600 (1974).

[21] E. Burstein, Phys. Rev. **93**, 632 (1954).

[22] T. S. Moss, Proc. Phys. Soc. London, Sect. B **67**, 775 (1954).

[23] L. F. J. Piper, T. D. Veal, C. F. McConville, H. Lu, and W. J. Schaff, Appl. Phys. Lett. **88**, 252109 (2006).

[24] A. Uedono, S. F. Chichibu, M. Higashiwaki, T. Matsui, T. Ohdaira, and R. Suzuki, J. Appl. Phys. **97**, 043514 (2005).

[25] J. Tersoff, Phys. Rev. B **32**, 6968 (1985).

[26] J. Robertson and B. Falabretti, J. Appl. Phys. **100**, 014111 (2006).

[27] S.-H. Wei and A. Zunger, Appl. Phys. Lett. **72**, 2011 (1998).

[28] C. F. Shih, N. C. Chen, P. H. Chang, and K. S. Liu, Jpn. J. Appl. Phys., Part 1 **44**, 7892 (2005).

[29] P. D. C. King, T. D. Veal, P. H. Jefferson, C. F. McConville, T. Wang, P. J. Parbrook, H. Lu, and W. J. Schaff, Appl. Phys. Lett. **90**, 132105 (2007).

[30] W. Mönch, J. Appl. Phys. **80**, 5076 (1996).

[31] S. H. Wei, X. L. Nie, I. G. Batyrev, and S. B. Zhang, Phys. Rev. B **67**, 165209 (2003).

[32] S.-H. Wei and A. Zunger, Phys. Rev. B **60**, 5404 (1999).

[33] S.-H. Wei and A. Zunger, Appl. Phys. Lett. **69**, 2719 (1996).

[34] S. X. Li, K. M. Yu, J. Wu, R. E. Jones, W. Walukiewicz, J. W. Ager III, W. Shan, E. E. Haller, H. Lu, and W. J. Schaff, Phys. Rev. B **71**, 161201(R) (2005).

[35] J. Wu, W. Walukiewicz, W. Shan, K. M. Yu, J. W. Ager III, S. X. Li, E. E. Haller, H. Lu, and W. J. Schaff, J. Appl. Phys. **94**, 4457 (2003).

[36] T. L. Tansley and C. P. Foley, J. Appl. Phys. **59**, 3241 (1986).

[37] P. D. C. King, T. D. Veal, C. F. McConville, F. Fuchs, J. Furthmüller, F. Bechstedt, P. Schley, R. Goldhahn, J. Schörmann, D. J. As, K. Lischka, D. Muto, H. Naoi, Y. Nanishi, Hai. Lu, and W. J. Schaff, Appl. Phys. Lett. **91**, 092101 (2007).

[38] K. M. Tracy, W. J. Mecouch, R. F. Davis, and R. J. Nemanich, J. Appl. Phys. **94**, 3163 (2003).

[39] T. D. Veal, P. H. Jefferson, L. F. J. Piper, C. F. McConville, T. B. Joyce, P. R. Chalker, L. Considine, H. Lu, and W. J. Schaff, Appl. Phys. Lett. **89**, 202110 (2006).